Published in final edited form as:
Chemistry. 2011 May 2; 17(19): 5350–5361. doi:10.1002/chem.201002162.

Phototriggering Electron Flow through Re^{I}-modified *Pseudomonas aeruginosa* Azurins

Ana María Blanco-Rodríguez[a], **Angel J. Di Bilio**[b], **Crystal Shih**[b], **Anna Katrine Museth**[b], **Ian P. Clark**[c], **Michael Towrie**[c], **Andrea Cannizzo**[d], **Jawahar Sudhamsu**[e], **Brian R. Crane**[e], **Jan Sýkora**[f], **Jay R. Winkler**[b], **Harry B. Gray**[b], **Stanislav Záliš**[f], and **Antonín Vlček Jr.**[a,f]

Jay R. Winkler: winklerj@caltech.edu; Harry B. Gray: hbgray@caltech.edu; Stanislav Záliš: zalis@jh-inst.cas.cz; Antonín Vlček: a.vlcek@qmul.ac.uk

[a]Queen Mary University of London, School of Biological and Chemical Sciences, Mile End Road, London E1 4NS, United Kingdom [b]Beckman Institute, California Institute of Technology, Pasadena, CA 91125, USA [c]Central Laser Facility, STFC Rutherford Appleton Laboratory, Chilton, Didcot, Oxfordshire OX11 0QX, United Kingdom [d]Laboratoire de Spectroscopie Ultrarapide, ISIC, FSB-BSP, Ecole Polytechnique Fédérale de Lausanne, CH-1015 Lausanne-Dorigny, Switzerland [e]Department of Chemistry and Chemical Biology, Cornell University, Ithaca, New York 14853, USA [f]J. Heyrovský Institute of Physical Chemistry, Academy of Sciences of the Czech Republic, Dolejškova 3, CZ-182 23 Prague, Czech Republic

Abstract

The $Re^{I}(CO)_3$(4,7-dimethyl-1,10-phenanthroline)(histidine-124)(tryptophan-122) complex, denoted Re^{I}(dmp)(W122), of *Pseudomonas aeruginosa* azurin behaves as a single photoactive unit that triggers very fast electron transfer (ET) from a distant (2 nm) Cu^{I} center in the protein. Analysis of time-resolved (ps-μs) IR spectroscopic and kinetics data collected on Re^{I}(dmp)(W122)AzM (M = Zn^{II} Cu^{II}, Cu^{I}; Az = azurin) and position-122 tyrosine (Y), phenylalanine (F), and lysine (K) mutants together with excited-state DFT/TDDFT calculations and X-ray structural characterization reveal the character, energetics, and dynamics of the relevant electronic states of the Re^{I}(dmp)(W122) unit and a cascade of photoinduced ET and relaxation steps in the corresponding Re-azurins. Optical population of Re^{I}(imidazole-H124)$(CO)_3$→dmp ^{1}CT states is followed by ~110 fs intersystem crossing and ~600 ps structural relaxation to a ^{3}CT state whose IR spectrum indicates a mixed $Re^{I}(CO)_3$,A→dmp/π→π*(dmp) character for aromatic amino acids A122 (A = W, Y, F) and $Re^{I}(CO)_3$→dmp MLCT for Re^{I}(dmp)(K122)AzCu^{II}. In a few ns, the ^{3}CT state of Re^{I}(dmp)(W122)AzM establishes an equilibrium with the $Re^{I}(dmp^{\bullet-})(W122^{\bullet+})$AzM charge-separated state, ^{3}CS, whereas the ^{3}CT state of the other Y, F, and K122 proteins decays to the ground state. In addition to this main pathway, ^{3}CS is populated by fs and ps W(indole)→Re^{II} ET from ^{1}CT and the initially "hot" ^{3}CT states, respectively. The ^{3}CS state undergoes a tens-of-ns $dmp^{\bullet-}$→$W122^{\bullet+}$ ET recombination leading to the ground state or, in the case of the Cu^{I} azurin, competitively fast (~30 ns over 1.12 nm) Cu^{I}→$W^{\bullet+}$ ET producing $Re^{I}(dmp^{\bullet-})$(W122)AzCu^{II}. The overall photoinduced Cu^{I}→Re(dmp) ET through Re^{I}(dmp)(W122)AzCu^{I} occurs over a 2 nm distance in <50 ns after excitation, the intervening fast ^{3}CT-^{3}CS equilibrium being the principal accelerating factor. No reaction was observed for the three Y, F, and K122 analogues. Although

Correspondence to: Jay R. Winkler, winklerj@caltech.edu; Harry B. Gray, hbgray@caltech.edu; Stanislav Záliš, zalis@jh-inst.cas.cz; Antonín Vlček, Jr., a.vlcek@qmul.ac.uk.

Supporting Information Available: Ns TRIR spectrum of Re^{I}(dmp)(Y)AzZn^{II}, DFT-calculated and experimental UV-vis absorption spectra of $[Re^{I}(phen)(W)]^{+}$ and Re^{I}(dmp)(W)AzCu^{II}, respectively, DFT-calculated IR spectra of the ground, ^{3}CT, and ^{3}CS states of $[Re^{I}(phen)(W)]^{+}$, ^{3}CT, and ^{3}CS electron density differences calculated with M06 and CAM-B3LYP functionals, comparison of calculated and experimental structural parameters of $[Re^{I}(phen)(W)]^{+}$ and Re^{I}(dmp)(W)AzCu^{II}, respectively, tables of TDDFT calculated vertical singlet and triplet electronic transitions of $[Re^{I}(phen)(W)]^{+}$.

the presence of Re(dmp)(W122)AzCu^{II} oligomers in solution was documented by mass spectrometry and phosphorescence anisotropy, kinetics data do not indicate any significant interference from intermolecular ET steps. The ground-state dmp-indole ππ interaction together with well-matched W/W$^{\bullet+}$ and excited-state Re^{II}(CO)$_3$(dmp$^{\bullet-}$)/Re^{I}(CO)$_3$(dmp$^{\bullet-}$) potentials, that result in very rapid electron interchange and ^{3}CT - ^{3}CS energetic proximity, are the main factors responsible for the unique ET behavior of Re^{I}(dmp)(W122)-containing azurins.

Introduction

Kinetics studies of long-range ET through metallolabeled mutants of a blue copper protein *Pseudomonas aeruginosa* azurin have greatly advanced our understanding of electron tunneling pathways through peptide β-strands[1-5] as well as at protein interfaces.[6] Theoretical analysis has revealed the roles of molecular fluctuations and multiple interfering tunneling pathways in tuning intraprotein ET rates in Ru-azurins.[7, 8]

Whereas oxidation of the azurin Cu^{I} center by electronically excited or oxidized metallolabels usually occurs on a μs-ms timescale,[1, 2] dramatic ET acceleration into the tens-of-ns range has been observed[9] in an azurin mutant where a tryptophan (W122) is placed next to a Re^{I}(CO)$_3$(dmp) label bound to the imidazole group of H124. (This Re-modified protein is denoted Re(dmp)(W)AzCu^{I} (dmp = 4,7-dimethyl-phenanthroline).)[10]- FOOTNOTE A sequential tunneling mechanism was proposed (Scheme 1), whereby the ^{3}CT-excited Re label is first reduced by the W122 indole group, followed by a Cu^{I}→W$^{\bullet+}$ ET, effectively splitting the ~2 nm ET pathway into two shorter steps.[9] The reaction mechanism involves several relaxation and ET events occurring on a timescales ranging from femto- to nanoseconds.

This work has raised important questions about the roles of the Re^{I}(CO)$_3$(dmp)/W122 unit and its electronic excited states in the ET mechanism. By replacing the Cu^{I} center with Cu^{II} or Zn^{II}, we cut out the long-range charge separation across the Re-labeled azurin (*i.e*. the 31 ns step in Scheme 1), isolate the reactive Re^{I}(dmp)(W) unit, and focus on the kinetics and mechanism of the primary ET step from W to the excited Re chromophore. Detailed structural, kinetics, and spectroscopic studies of Re^{I}(dmp)(W)AzM (M = Zn^{II}, Cu^{II}, and Cu^{I}) using ps-ns time-resolved IR and emission spectroscopy, combined with a theoretical (TD-DFT) excited-state analysis, provide a comprehensive picture of Re^{I}(dmp)(W) photobehavior and single out factors that make this unit a unique ultrafast ET phototrigger. It emerges that the ET-accelerating role of the tryptophan intermediate goes well beyond the simple splitting of the ET path, with interesting implications for long-range hopping in biological systems as well as for the design of new molecular schemes for photoinduced charge separation.

Experimental

Materials

Re^{I}(dmp)(A)AzCu^{II} (A = W, Y, F) were prepared and handled as described previously[9, 11] and in the Supplementary Information. The Re^{I}(dmp)(A)AzZn^{II} samples were made from the corresponding apoprotein by Zn^{II} addition. TRIR experiments were performed in 50 mM Na/KP$_i$ buffer in D$_2$O (pD ≅ 7.2) at 21 °C. Emission experiments were performed in H$_2$O, 50 mM NaP$_i$ (pH ≅7.1) at 21 °C. Reduction to Re^{I}(dmp)(A)AzCu^{I} was accomplished by slow additions of a concentrated solution of sodium dithionite (Aldrich) in 0.5-1.0 μL steps into an azurin solution under nitrogen atmosphere until it turned colorless. TRIR experiments were thus performed in the presence of a small excess of dithionite. The

crystallographic structure determination of Re^{I}(dmp)W122AzCu^{II} was reported previously,[9] and the coordinates are deposited in the protein data band with id 2i7o.

Time-resolved infrared (TRIR) and luminescence spectroscopy

TRIR measurements and procedures have been described in detail.[12, 13] In short, for ps experiments (0 – 2 ns), the sample solution was excited at 400 nm, using frequency-doubled pulses from a Ti:sapphire laser of ~150 fs duration (FWHM) and *ca*. 3 μJ energy, focused at an area ~200 μm in diameter. TRIR spectra were probed with IR (~150 fs) pulses obtained by difference-frequency generation. The IR probe pulses cover a 150-200 cm^{-1} spectral range. For ns-μs measurements, the sample was pumped with 355 nm, 0.7 ns FWHM, and probed with electronically synchronized 150 fs IR pulses.[14] The sample solutions were placed in a round dip *ca*. 0.75 mm deep, drilled into a CaF_2 plate and tightly covered with a polished CaF_2 window. The cell was scanned-rastered across the area of the dip in two dimensions to prevent laser heating and decomposition of the sample. FTIR spectra measured before and after the experiment demonstrated sample stability.

Emission lifetime and time-resolved anisotropy measurements were performed using time-correlated single-photon counting (TCSPC) on an IBH 5000 U instrument equipped with a cooled Hamamatsu R3809U-50 microchannel plate photomultiplier, following the procedures described previously.[15] The samples were excited at 370 nm with an IBH NanoLED-11 diode laser (FWHM 100 ps, 500 kHz repetition rate).

TRIR data analysis

TRIR data were analyzed using singular value decomposition (SVD) followed by fitting to a multiexponential kinetics equation[16, 17] implemented (EPFL, Switzerland) in the WaveMetrics IGOR Pro software tool. In brief, this analysis allows us to separate the stochastic noise from the signal $\Delta A(\tilde{\nu}, t)$ and express the latter in terms of P spectral $\varepsilon_l(\tilde{\nu})$ and temporal $c_l(t)$ components:

$$\Delta A(\tilde{\nu}, t) = \sum_{l=1}^{P} \varepsilon_l(\tilde{\nu}) c_l(t) \tag{1}$$

Where $\Delta A(\tilde{\nu}, t)$ is the IR difference absorbance measured at time delay t and wavenumber $\tilde{\nu}$. The $c_l(t)$ components are then fitted simultaneously to the appropriate kinetics equation. Herein we used a multiexponential kinetics model, eq. 2.

$$c_l(t) = \left(\sum_{k=1}^{n} A_l e^{-t/\tau_k} \right) \otimes e^{-(1.6 - t/\Delta_{IRF})^2} \tag{2}$$

where a common set of lifetimes (τ_k) describes the dynamic behavior of all the temporal components. This allows us to rewrite eq. 2 as follows:

$$\Delta A(\tilde{\nu}, t) = \sum_{k=1}^{n} DAS_k(\tilde{\nu}) e^{-t/\tau_k} \otimes e^{\left[-\left(\frac{t}{0.6 * \Delta_{IRF}} \right)^2 \right]} \tag{3}$$

where $DAS_k(\tilde{\nu})$ is the Decay Associated Spectrum describing the spectral contribution of the respective decay component with a time constant τ_k. The last term describes convolution with the Gaussian instrument response function. Δ_{IRF} = 1 ps (or 1 ns) was used for ps (or ns)

experiments. Elementary rate constants were extracted from an analytical solution of the differential equations describing the kinetics model depicted in Scheme 1.[9]

Electronic structure calculations

The electronic structure of the model fragment $[Re^{I}(CO)_3(phen)(W)]^+$ (Figure 1 bottom) was calculated by density functional theory (DFT) methods using the Gaussian 09 program package,[18] employing the hybrid functionals PBE0[19, 20], M06[21] and long-range corrected CAM-B3LYP[22]. For H, C, N, O atoms, 6-31g* polarized triple - ζ basis sets[23] were used for geometry optimization and vibrational analysis and cc-pvdz correlation consistent polarized valence double-ζ basis sets[24] were utilized in TDDFT calculations. Quasirelativistic effective core pseudopotentials and a corresponding optimized set of basis functions were employed for Re.[25] The solvent was described by a conductor-like polarizable continuum model (CPCM).[26] Electronic transitions were calculated by the time-dependent DFT (TDDFT) method at the ground-state geometry optimized with solvent correction. The structure of the lowest triplet excited state a^3A was optimized by UKS calculations. The triplet excited state calculation is in satisfactory agreement with experimental TRIR spectra in the *ν*(CO) region. The electron density difference plots were drawn using the GaussView program. $[Re^{I}(CO)_3(phen)(W)]^+$ was chosen as a computational model instead of $[Re^{I}(CO)_3(dmp)(W)]^+$ because of a better convergence of UKS optimizations of some of the excited-state structures. Ground-state PBE0 calculations of $[Re^{I}(CO)_3(dmp)(W)]^+$ and $[Re^{I}(CO)_3(phen)(W)]^+$ yield very similar structural parameters (Table S1) as well as excitation energies (Table S2a-b), closely matching the experimental values.

Results

Crystal structures

The crystal structure of Re^{I}(dmp)(W)AzCu^{II} (Figure 1) shows the Re and Cu atoms 19.4 Å apart. W122 lies between them, 11.2 Å from Cu and 8.9 Å from Re, as measured to the indole C^{γ} atom. The dmp and W122 aromatic rings slightly overlap, with one dmp methyl group projecting directly over the indole ring; the planes of the respective π-systems making a 20.9° angle. The average separation of atoms on the overlapped six-membered rings is 3.82 Å, whereas the W122 indole and the H124 imidazole edges are separated by 4.1 Å. Comparison of the structures of Re^{I}(dmp)(W)AzCu^{II} and Re^{I}(phen)(K)AzCu^{II} in Figure 1 shows that the orientations of the $Re(CO)_2$(N,N) units (N,N = dmp, phen) relative to the peptide chain and the im(H124) ligand differ by close to 90°. The H124 imidazole ring and the equatorial $Re(CO)_2$(dmp) plane in Re^{I}(dmp)(W)AzCu^{II} adopt an unusual orientation, whereby the imidazole plane lies close (16°) to the symmetry plane of the equatorial $Re(CO)_2$(dmp) moiety, bisecting the plane of the dmp ligand (Figures 1, 2). In contrast, the plane of the axial ligand is oriented perpendicularly to the symmetry plane, bisecting the equatorial OC-Re-N angles in Re^{I}(phen)(K)AzCu^{II} (Figure 1 top), other structurally characterized Re-azurins[2, 15, 27] except Re^{I}(phen)(H83)AzCu^{II}, the small-molecule analogue[28] $[Re^{I}(im)(CO)_3(phen)]^+$, and various complexes $[Re^{I}(R\text{-}py)(CO)_3(N,N)]^+$ (N,N = phen, bpy).[29-33]

Figure 2 shows that Re^{I}(dmp)(W)AzCu^{II} is a dimer with two-fold symmetry in the crystal; the dominant interactions between neighboring molecules involve the dmp ligands, which cover each other on their outside faces. Unlike the hooking interactions that interdigitate the phen moieties in Re^{I}(dmp)(H107)AzCu^{II} (PDB code 1i53)[11, 15, 34] and Re^{I}(phen)(K)AzCu^{II} (PDB code 2i7s) [15] crystals, the Re^{I}(dmp)(W)AzCu^{II} dmp ligands are not constrained by the axial H124 and thus can align to a greater extent. One six-membered dmp ring directly stacks with one from a neighboring complex. A 4-centered weakly interacting

W122···dmp···dmp···W122 stack is apparent in the dimer structure. The $Re(CO)_3$ unit makes van der Waals contacts with the peptide chains: one equatorial carbonyl ligand abuts the methyl side chain of Ala53, whereas the other is within 3.6 Å of the Gln107 side chain. The axial carbonyl points towards an adjacent molecule in the lattice and is within 4.0 Å of the sulfur atoms of both Met109 and Met56 side chains. The axial carbonyl would point away from the protein surface in a solvated monomer in solution.

Solution structure

Solution IR spectra in the region of CO stretching vibrations, *ν*(CO) (Figure 3), show the same pattern for all three Re^{I}(dmp)(A)AzM^{II}: a sharp band due to the in-phase A'(1) vibration at 2028 cm^{-1}; and a broad band at *ca*. 1917 cm^{-1} that corresponds to quasidegenerate out-of-phase A'(2) and equatorial asymmetric A" vibrations. In the IR spectrum of Re^{I}(phen)(K)AzCu^{II}, the A'(2) and A" bands are split: 1907 and 1924 cm^{-1}, respectively. (Symmetry labels assume C_s local symmetry; the assignment is based on previous work[35, 36] and DFT calculations reported below.) We conclude from the IR spectra that all the Re(dmp)(A)AzM^{II} proteins containing a 122 aromatic amino acid have the same Re-site solution structure, different from Re^{I}(phen)(K)AzCu^{II}. The A'(2)+A" bandshapes indicate that the three CO ligands reside in a much more diverse environment in Re^{I}(phen)(K)AzCu^{II} than Re^{I}(dmp)(A)AzM^{II}. Accordingly, the crystal structures show large asymmetry between the two equatorial COs in Re^{I}(phen)(K)AzCu^{II}, where one equatorial CO is directed at Lys122 and Gln107 and the other is solvated, unlike Re^{I}(dmp)(W)AzCu^{II}, where both equatorial COs point against an aliphatic side chain of the same molecule.

Mass spectra (LILBID-MS) obtained from aqueous (20 mM NaP_i, pH ~7.0) solutions of Re^{I}(dmp)(W)AzCu^{II} clearly show the presence of higher azurin oligomers, especially at higher concentrations, 1-3 mM.[37] Oligomers also are indicated by relatively high values of protein rotation times T_2 that were determined from the biexponential emission anisotropy decay of Re^{I}(dmp)(W)AzCu^{II} in 20 mM NaP_i, pH ~7.1 (3.7 mM: T_1 = 5.1±4.3 ns (18%), T_2 = 31.5 (82%); 0.37 mM: T_1 = 5.1±3.4 ns (36%), T_2 = 16.5±3.5 ns (64%)) and Re^{I}(dmp)(Y)AzZn^{II} in 50 mM Na/KP_i, D_2O, pD ~7.1 (4.4 mM: T_1 = 4.8±0.7 ns (32%), T_2 = 50±2 ns (68%); 0.44 mM: $T_1 \cong$ 1 ns, T_2 = 30±1 ns (45%)). At the same time, the relatively large T_1 values are attributable to slower Re(dmp)-chromophore motions relative to the peptide than those in Re-azurins that do not contain an aromatic amino acid next to the Re label.[15]

Photoinduced electron transfer: TRIR spectra and emission decay

TRIR spectroscopy is a technique-of-choice to study excited-state behavior of metal carbonyls since the CO stretching vibrations sensitively respond to changes in electronic and molecular structure[38] as well as to relaxation dynamics of the molecular environment following photoexcitation.[15] The IR spectra were measured at selected ps time delays after 400 nm excitation directed to the low-energy part of the $Re(CO)_3$→dmp MLCT absorption band, Figure S2-bottom. By exciting into the red part of band we have avoided additional vibrational excitation. Excitation at 355 nm close to the MLCT band maximum was used (for instrumental reason) in nanosecond experiments. Spectra measured at 355 and 400 nm overlapped in the 1-2 ns time range where either instrumental setup can be used, excluding any specific excitation-wavelength effects on the nature of the populated excited states and their reactivity.

For Re^{I}(dmp)(Y)AzZn^{II}, Re^{I}(dmp)(Y)AzCu^{II}, and Re^{I}(dmp)(F)AzCu^{II}, TRIR spectra show only the negative bleach bands due to ground-state depletion and three upshifted bands attributable[15, 27, 35, 38-43] to a $Re(CO)_3$→dmp ^{3}CT state, approximately described as $Re^{II}(dmp^{\bullet -})$(A)AzM (Figures 4 and S1). The excited-state IR features undergo a small ps-ns upshift due to relaxation processes (Figure S1).[15] On a longer timescale, the transient and

bleach bands decay with virtually identical kinetics (Figure S1), demonstrating that the ^{3}CT state decays directly to the ground state. A ^{3}CT lifetime of 1.36±0.17 μs determined (TRIR) for Re^I(dmp)(Y)AzZn^{II} is close to the Re^I(dmp)(F)AzCu^I emission lifetime of 1.3 μs.[9] Re^I(dmp)(F)AzCu^{II} (1 mM in H_2O, 50 mM NaP_i pH ≅ 7.1) shows triexponential emission decay with lifetimes of 3.5±0.3 (12%), 76.0±2.6 (32%), and 344±10 ns (55%). The longest decay component corresponds to the ^{3}CT population decay, whereas structural relaxation dynamics and/or oligomerization could account for the shorter kinetics components. The shorter excited-state lifetime in Cu^{II} (as compared to Zn^{II}) azurins is attributed to ^{3}CT→Cu^{II} energy transfer,[44-46] as dmp$^{\bullet-}$→Cu^{II} ET is excluded by the absence of TRIR signals that would accompany the production of $Re^{II}(CO)_3$(dmp). (Oxidation of excited Re-label (E' ≅ −0.9 V)[28] by Cu^{II} in azurin (+0.31 V) is thermodynamically possible but presumably slow because of long distance and large reorganization energy on the Re side.)

TRIR spectra (Figure 5) of Re^I(dmp)(W)AzM (M = Zn^{II}, Cu^{II}, Cu^I) exhibit the typical three upshifted bands due to the ^{3}CT state, together with a broad band at ~1885 cm^{-1} and a sharp band at ~2004 cm^{-1} that are assigned to the A"+A'(2) and A'(1) vibrations, respectively, of the W(indole)→$Re(CO)_3$(dmp) ^{3}CS state, Re^I(dmp$^{\bullet-}$)(W$^{\bullet+}$)AzM. (Hereinafter, these sets of IR bands will be abbreviated ^{3}CT and ^{3}CS bands, respectively.) The ^{3}CS band assignment is based on the similarity with IR spectra of [Re^I(*N*-L)$(CO)_3$(bpy$^{\bullet-}$/phen$^{\bullet-}$)] (*N*-L = nitrogen-donor ligand such as MeCN, picoline or pyridine) generated either electrochemically[47-49] or photochemically[38, 48, 50, 51] by intramolecular electron transfer. Whereas the spectral pattern consisting of ^{3}CT and ^{3}CS bands is very similar for all three Re^I(dmp)(W)AzM (M = Zn^{II}, Cu^{II}, Cu^I) derivatives, the kinetics and ^{3}CS yields depend on M. Temporal evolution of TRIR spectra of the individual Re^I(dmp)(W)AzM systems in ps and ns-μs time ranges are described in terms of exponential lifetimes and their corresponding decay associated spectra (DAS), eq. 3, obtained by SVD analysis/global fitting. Comparable kinetics data were obtained on different samples of each azurin using variations of the fitting procedure. For M = Cu^{II} and Cu^I, the results obtained on 3-4 and 1.7 mM samples are the same within experimental accuracy. The resultant TRIR and emission lifetime data are summarized in Table 1.

Re^I(dmp)(W)AzZn^{II}—The IR bands of the ^{3}CT state are fully developed within the experimental time resolution of ~1 ps, undergoing relaxation-related dynamic upshifts in the first ~1.5 ns, (Figure 5). The ^{3}CS band at ~1885 cm^{-1} is also apparent at 1-2 ps, increasing in intensity by ~60% during the first 30-50 ps.

In the ns range, formation of both ^{3}CT and ^{3}CS transients appears to be complete within the 0.7 ns excitation pulse, followed by biexponential decay with low-amplitude 18 ns and principal 157 ns kinetics components, the former involving some 1885 cm^{-1} band-shape changes (Figure 6). A very small ^{3}CT population persists on a longer timescale, after the ^{3}CS bands had disappeared (see the 500 and 1000 ns experimental traces and the 1300 ns DAS that copies the ^{3}CT spectrum, Figure 6).

Re^I(dmp)(W)AzCu^{II}—Picosecond TRIR spectra (Figure 7, left panel) show both the ^{3}CT and ^{3}CS states being formed within the first ps after excitation. The temporal evolution on the ps timescale consists of band shifts, width narrowing and intensity variations that make it hard to distinguish population changes from relaxation effects. To address this matter, we have performed separate SVD/global fitting analyses in the full spectral range where the relaxation strongly manifests itself by spectral shifts above ~1980 cm^{-1}, and in the 1843-1972 cm^{-1} range, where population changes prevail. These analyses have identified 4-5 ps and ~110 ps upshifts of the ^{3}CT A" and A'(1) bands. The latter component slows to 220-300 ps when fitted over the whole spectral range. The negative DAS in the region of the ^{3}CS 1885 cm^{-1} band and at ~2004 cm^{-1}, together with the relatively large positive DAS

amplitudes corresponding to hot ^{3}CT bands indicate that ps relaxation processes are accompanied by conversion of the ^{3}CT state to ^{3}CS, whose IR features become more pronounced in the 100-300 ps range. On the nanosecond scale (Figure 7, right panel), there is a major 4-8 ns ^{3}CS rise / ^{3}CT decay followed by a common 40-60 ns decay of both ^{3}CS and ^{3}CT states. Whereas ^{3}CT bands decay completely, a weak long-lived (1000-1500 ns) ^{3}CS signal persists. In addition to intensity changes, the ~1885 cm^{-1} ^{3}CS band undergoes a small upshift to ~1992 cm^{-1} that is complete in 150-200 ns.

Re(dmp)(W)AzCu^{I}—TRIR spectra (Figure 8) show qualitatively the same pattern as that of the Cu^{II} species, albeit with much stronger ^{3}CS bands. The ^{3}CT state and part of the ^{3}CS population are formed within the 1 ps experimental resolution. Further picosecond spectral time evolution consists of a 3-4 ps upshift of the ^{3}CT bands, followed by a 40-100 ps ^{3}CT upshift and small decay, combined with a ^{3}CS rise. On the nanosecond scale, the ^{3}CS rise and ^{3}CT decay continue with time constants of 1.6 ns (determined from the ps experiment), 8 ns (major) and 27 ns (minor). The latter is manifested by a rise mostly of the high-energy side of the 1885 cm^{-1} band and a ^{3}CT decay. The 27 ns process leaves only the ^{3}CS product that decays with minor 330 ns and major 3.6 μs kinetics components. As in the case of the Cu^{II} species, there is a small upshift and shape-change of the 1885 cm^{-1} ^{3}CS band after 150-200 ns.

TRIR spectra also were measured from solutions of Re(dmp)(Y)AzZn^{II}, Re(dmp)(Y)AzCu^{II} and Re(dmp)(F)AzCu^{II} in the presence of a large excess of $Na_2S_2O_4$. TRIR bands of Re^{I}(dmp$^{\bullet-}$)(Y)AzM (M = Zn^{II}, Cu^{I}) are formed at ~1885 and 2004 cm^{-1} with lifetimes of hundreds-of-ns. The absence of such long rise kinetics in TRIR measurements on Re(dmp)(W)AzCu^{I} excludes any possible contamination from ^{3}CT quenching by sodium dithionite in solution.

Electron transfer kinetics and mechanism

The spectroscopic and kinetics data for Re^{I}(dmp)(W)AzM are consistent with the mechanism[9] outlined in Scheme 1 for Re^{I}(dmp)(W)AzCu^{I}. The long-range ET is shut out in the case of M = Zn^{II}, Cu^{II} ($k_5 = k_6 = 0$), restricting the ET activity to the Re^{I}(dmp)(W) moiety. The kinetics data (Table 1) were analyzed using the model[9] shown in Scheme I, revealing the time ranges of individual reaction steps and estimating values of the ^{3}CT-^{3}CS equilibrium constant *K*.

Re^{I}(dmp)(W)AzZn^{II}—The ^{3}CS state is produced in <1 and <50 ps (Figures 5, S1). No ^{3}CT / ^{3}CS equilibration is seen on the ns timescale, indicating that ^{3}CS formation occurs only from ^{1}CT and unequilibrated ^{3}CT states. By deconvoluting the ^{3}CT and ^{3}CS spectra and comparing their ratio with Re^{I}(dmp)(W)AzCu^{II}, *K* was estimated as 0.34. The major 157 ns decay component corresponds to the ^{3}CS decay that is in a fast equilibrium with the long-lived (1.36 μs) ^{3}CT state. The minor 18 ns component probably reflects conformational changes in the ^{3}CS state since the corresponding DAS indicates shape changes of the ~1885 cm^{-1} band.

Re^{I}(dmp)(W)AzCu^{II}—Using the time constants from Figure 7, we estimate *K* as 1.6. The 4-8 ns lifetime (Table 1) reflects ^{3}CT / ^{3}CS equilibration, k_3+k_4. ^{3}CS decays (together with ^{3}CT) with a ~60 ns lifetime that is related to k_8. The small residual ^{3}CS signal (apparent in Figure 7, the 1000 ns spectrum and the 1070 ns DAS) that decays with a 1-1.5 μs lifetime is tentatively attributed to the deprotonated species Re^{I}(dmp$^{\bullet-}$)(W$^{\bullet}$)AzCu^{II} produced by a slow side reaction from the ^{3}CS state Re^{I}(dmp$^{\bullet-}$)(W$^{\bullet+}$)AzCu^{II}. W$^{\bullet+}$ deprotonation is expected to occur with a time constant of 100-200 ns.[52] Consistent with

this expectation, the ~1885 cm^{-1} ^{3}CS band reshapes and shifts to ~1990 cm^{-1} between 50 and 150 ns.

Re^{I}(dmp)(W)AzCu^{I}—Empirical rate constants determined herein by SVD/global fitting (Table 1) of the TRIR data generally agree with the results of our previous analysis (Scheme I).[9] The IR spectra of the ^{3}CS state and the ET product are very similar, belonging to the same chromophore, $Re^{I}(CO)_3(dmp^{\bullet-})$, albeit in a different protein environment. The main 1.6 ns kinetics component corresponds to ^{3}CT/^{3}CS equilibration k_3+k_4 ($K \cong 3$)[9] whereas the 8-9 ns lifetime probably belongs to the same process in a less reactive conformer or an oligomer. The ~27 ns kinetics component is related to $Cu^{II} \rightarrow W^{\bullet+}$ ET in the ^{3}CS state (k_5), since the corresponding DAS indicates reshaping of both ^{3}CS bands. The *ca*. 330 ns lifetime could be related to structural changes of the $Re^{I}(dmp^{\bullet-})$(W)AzCu^{II} product. The ground state is regenerated by 3.1-3.6 μs $dmp^{\bullet-} \rightarrow Cu^{II}$ ET (k_6) that is exergonic by *ca*. 1.8 eV

Re-label excited-state character and dynamics: TRIR spectra

The Re-chromophore in Re^{I}(dmp)(A)AzM shows the typical ^{3}CT broad emission band peaking at 540-550 nm and three excited-state ν(CO) IR bands that are shifted to higher wavenumbers relative to the ground-state bands (Figures 4-8 and S1). The A" and A'(2) bands become well separated upon excitation, shifted from their common ground-state value of 1917 cm^{-1} to *ca*. 1960 and 2014 cm^{-1}, respectively, as observed for other Re^{I}-azurins and Re^{I} carbonyl-diimine complexes.[15, 27, 35, 38-43] The A'(1) bands of Re(phen)(K)AzCu^{II} and Re(dmp)(K)AzCu^{II} shift by +38.5 and ~25 cm^{-1}, respectively, on going from the ground state to the relaxed ^{3}CT excited state, indicating a smaller degree of $Re(CO)_3 \rightarrow$N,N charge separation for N,N = dmp. Further differences concern the dynamical behavior of the A'(1) band after excitation (Figure 9). For Re^{I}(phen)(K)AzCu^{II}, A'(1) undergoes an "instantaneous" (i.e. <1 ps) shift of +9.4 cm^{-1}, followed by a triexponential dynamical upshift with time constants of 2, 7.8, and 539 ps, and a total amplitude of +29 cm^{-1}; the slowest (539 ps) component corresponds to structural motions relocating the Re^{I}-chromophore relative to the peptide chain.[15] The excited-state A'(1) IR band of Re^{I}(dmp)(K)AzCu^{II} is much broader, the "instantaneous" shift is slightly negative and the dynamic blue shift is still apparent between 2 and 3 ns, although it cannot readily be quantified. The Re-azurins containing position-122 aromatic amino acids show a common excited-state IR-pattern (Figure 9) that is different from that of Re^{I}(dmp)(K)AzCu^{II} and other Re-azurins.[15] The excited-state A'(1) band partly overlaps with the bleach and tails toward higher energies. At 1-2 ps after excitation, the A'(1) band is shifted to lower energies by at least -12 cm^{-1}. This negative "instantaneous" shift is followed by a dynamic upshift across the bleach region that is apparent until ~2 ns. The band maximum of the relaxed excited state is upshifted from the ground-state position by only 8-10 cm^{-1} for W122 and 10-13 cm^{-1} for Y122 and F122. The relatively small A'(1) upshift points to a smaller $Re(CO)_3 \rightarrow$dmp MLCT contribution to the excited state if an aromatic amino acid is placed next to the Re chromophore; this conclusion is further supported by DFT and TD-DFT calculations below.

Re-label excited-state character and dynamics: Electronic structure calculations

DFT calculations were performed on a model peptide fragment $[Re^{I}(phen)(W)]^+$ with L125 and M121 replaced by CH_3NH- and $CH_3C(O)$-, respectively (Figure 1, bottom). The H_2O solvent was described by a continuum dielectric model CPCM. Calculations with three different functionals (PBE0, M06, and CAM-B3LYP) were compared, each of which provides an optimized $[Re(phen)(W)]^+$ structure that represents the relevant part of the protein (Figure 1, Table S1). However, M06 overestimates the ground-state W(indole)-phen interaction, giving distances and the angle between the indole and phen planes too small. The long-range corrected B3LYP functional (CAM-B3LYP) reproduces well the ground-state structure (Table S1) and models the ^{3}CS state in accordance with the M06 result

(Figure S5), but predicts that the lowest allowed electronic transitions are at much higher energies than observed in the experimental absorption spectrum.

According to PBE0, the three LUMOs are localized on phen, while HOMO and HOMO-1 are W122 indole-ring π orbitals (Figure 10). Re dπ orbitals occur slightly lower in energy, as HOMO-2, which contains a large H124-imidazole π contribution; and HOMO-3. The orbitals HOMO-4,5 are π peptide (W122) orbitals.

TDDFT positions of singlet electronic transitions of $[Re^{I}(phen)(W)]^{+}$ are summarized in Tables S2, S4, and S5. The simulated and experimental spectra are shown in Figure S2. The two lowest transitions calculated (PBE0) at 465 ($b^{1}A$) and 424 nm ($c^{1}A$) have W(indole) →phen charge transfer character, originating in HOMO→LUMO,LUMO+1 excitations, as documented by the accompanying electron-density change shown in Figure 11 (Figure S5) for PBE0 (M06 and CAM-B3LYP) results. Oscillator strengths of these two transitions are very low (Table S2), precluding observation in the spectrum. Other weak W(indole)→phen transitions were calculated around 380 nm. Two intense transitions from HOMO-2,3 to LUMO and LUMO+1 calculated at 350 ($g^{1}A$) and 335 nm ($i^{1}A$) give rise to the experimentally observed broad 300-400 nm shoulder. Calculated electron-density differences (Figure 11) demonstrate their respective predominant $Re^{I}(CO)_{3}$→phen MLCT and mixed Re^{I}(imidazole)$(CO)_{3}$→phen MLCT/LLCT characters. Both these transitions are excited by 355 and 400 nm laser pulses in the time-resolved spectral experiments. Another intense, predominantly ^{1}CT, transition was calculated at 329 nm.

TDDDFT calculation at the ground-state geometry reveals two nearly degenerate triplet states: the charge-transfer state, ^{3}CT, has major Re^{I}→phen, and minor imidazole→phen, W(indole)→phen and π→π*(phen) contributions, whereas the charge-separated state, ^{3}CS, has a W(indole)→phen character, $^{3}[Re^{I}(phen^{\bullet-})(W^{\bullet+})]^{+}$ (Figure 12, top). UKS (PBE0/CPCM-H_2O) triplet-state structural optimization identifies the lowest relaxed triplet excited state of $[Re^{I}(phen)(W)]^{+}$ as ^{3}CT, demonstrated by the spin-density distribution (Figure 12). Predicted ν(CO) shifts between the ^{3}CT and ground and excited states of +42 (A"), +75 (A'(2)), and +8 (A'(1)) cm^{-1} agree well with the experimental values of +40, +94, and ≤+10 cm^{-1} (Figure S3). The unusually small A'(1) ν(CO) shift is caused by the very small CO electronic depopulation that is mainly restricted to the axial CO (Figure 12). The extent of $Re^{I}(CO)_{3}$→phen charge transfer in the ^{3}CT state is limited by two effects: admixture of the ππ*(phen) intraligand excitation and partial charge transfer from the W122 indole ring. The similarity of Re^{I}(dmp)(A=W,F,Y)AzM TRIR spectra (Figure 9) suggests that phenol and phenolate groups also donate electron density to dmp in the ^{1}CT excited states of Re(dmp)(F)AzM and Re(dmp)(Y)AzM, respectively. UKS (M06/CPCM-H_2O) predicts that ^{3}CS of a W(indole)→phen character, $^{3}[Re^{I}(phen^{\bullet-})(W^{\bullet+})]^{+}$ (Figure 12), will be the lowest triplet, allowing us to optimize its structure and perform vibrational analysis. The ^{3}CS A"+A'(2) ν(CO) vibrations (M06/H_2O, Figure S4) are downshifted from ground-state values by -30 and -23 cm^{-1}, respectively, because of the increased π electron density on the phen ligand. Accordingly, TRIR spectra show bands at ~1885 (A"+A'(2)) and ~2004 cm^{-1} (A'(1)), that is ~33 and 26 cm^{-1} lower than corresponding ground-state bands. The sensitivity of the electronic structure of the lowest triplet states to the computational details is in line with the experimentally determined energetic proximity of the Re^{I}(dmp)(W122)$AzCu^{I}$ ^{3}CT and ^{3}CS states, ~0.028 eV.[9] The good match between experimental and calculated excited-state IR spectra demonstrates that UKS PBE0 and M06 calculations in water provide good models for the ^{3}CT and ^{3}CS states, respectively.

Discussion

The $Re^{I}(CO)_3$(dmp)(H124)(W122) unit of the azurin mutant emerges from this study as an electronically coupled active site that can be regarded as a single photoactive unit. The X-ray crystal structure (Figure 1) clearly demonstrates an interaction between the nearly parallel W(indole) and dmp rings that is strong enough to rotate the $Re^{I}(CO)_3$(dmp) label relative to its position in Re^{I}(dmp)(K)AzCu^{II} by ~90° and change the orientation of the H124 imidazole ligand relative to the $Re^{I}(CO)_3$(dmp) symmetry plane. DFT calculations and both ground- and excited-state IR spectra indicate that the intramolecular W(indole)-dmp interaction persists in solution. Similar interaction occurs between dmp and F122 (or Y122) in Re^{I}(dmp)(F or Y)AzM. Although azurins, including Re(dmp)(W)AzCu^{II}, form oligomers in solutions,[37] the kinetics data can be interpreted in terms of intramolecular ET and relaxation steps only. Intraprotein ET is much faster than ET across protein-protein interfaces in oligomers, especially when the proteins are bound by nonspecific forces, as indicated[37] by LILBID mass spectra. Intermolecular ET would not be competitive even if the indole-dmp-dmp-indole interaction found in Re(dmp)AzCu^{II} dimers in crystals (Figure 2) were preserved in an oligomer core, as each dmp ligand is coupled to an indole of the same azurin molecule, being separated from that of the second molecule by another Re(dmp) unit.

Photoinduced charge separation producing the $Re^{I}(dmp^{\bullet-})(W^{\bullet+})$AzM ^{3}CS state involves several ET steps that occur on timescales ranging from femtoseconds to a few tens of ns (Scheme 1, Table 1). The ET reactivity can be understood in terms of the electronic structure, energetics and relaxation dynamics of electronic excited states of Re^{I}(dmp)(W). Optical excitation populates ^{1}CT excited states ($Re^{II}(dmp^{\bullet-})$(W), Figure 11) that undergo intersystem crossing with a time constant of *ca*. 110 fs,[16, 17, 53] producing a hot ^{3}CT state. The ~110 fs ^{1}CT lifetime allows for ultrafast exergonic W→Re^{II} ET to the ^{1}CS state, followed by fs intersystem crossing to ^{3}CS. This pathway is responsible for sub-ps ^{3}CS formation, observed by TRIR. (Direct optical excitation into W→dmp ^{1}CS states is improbable because of the very low oscillator strengths of corresponding transitions: Table S2, Figure S2.) The ^{3}CT state is initially "hot": it is both vibrationally excited and in an unequilibrated solvent and protein environment.[15] Relaxation (complete in 1-2 ns, as follows from the dynamical shift of the excited-state A'(1) ν(CO) band) involves a multitude of structural movements optimizing electrostatic interactions between the excited Re-label, the peptide and solvent molecules.[15] Concomitantly with structural relaxation of the Re-site, the hot ^{3}CT state undergoes W→$Re^{II}(dmp^{\bullet-})$ ET to the ^{3}CS state $Re^{I}(dmp^{\bullet-})(W^{\bullet+})$ in tens to hundreds of ps, slowing to ~1 ns upon ^{3}CT relaxation. The relaxed ^{3}CT state is the principal precursor of charge separation. Electronic interaction between W(indole) and dmp in the predominantly Re→dmp/$\pi\pi^*$(dmp) ^{3}CT state is evident from calculated electron-density changes and excited-state spin-density distribution that partly extend over the W(indole) moiety (Figure 12). The ^{3}CT to ^{3}CS conversion can be viewed either as a W(indole)→$dmp^{\bullet-}$→Re^{II} electron-density shift or a W→Re^{II} ET mediated by $dmp^{\bullet-}$ (and its $\pi\pi$ interaction with the indole). An alternative ET pathway through peptide bonds is less likely because of much longer length and negligible electronic involvement of peptide and imidazole orbitals in the ^{3}CT state (Figures 10, 12). DFT calculations show that the relaxed ^{3}CT and ^{3}CS states are nearly isoenergetic. Accordingly, the kinetics analysis points to an equilibrium between these two states, with ^{3}CS only 0.028 (0.012) eV below ^{3}CT for Cu^{I} (Cu^{II}), whereas ^{3}CS is 0.027 eV above ^{3}CT for Zn^{II}. The $Re^{I}(dmp^{\bullet-})(W^{\bullet+})$AzM ^{3}CS state decays to the ground state by $dmp^{\bullet-}$→$W^{\bullet+}$ charge recombination that takes place with a 30-60 ns time constant for Cu^{II} or Cu^{I} and ~160 ns for Zn^{II}. This is a highly exergonic process (2.0-2.5 V) occurring in the Marcus inverted region. The ET and relaxation dynamics within Re^{I}(dmp)(W) are similar for Cu^{I} and Cu^{II}, the equilibrium constant *K* being slightly larger for Cu^{II} (3) than Cu^{I} (1.6). Re^{I}(dmp)(W)Zn^{II} is distinctly different, since

the ^{3}CS state is formed only by ultrafast processes in a close-to-equilibrium ratio. W→Re^{II} ET (^{3}CT→^{3}CS) is slightly endergonic ($K \cong 0.34$), in contrast to the Cu^I and Cu^{II} energetics. The different Zn^{II} azurin behavior could be attributable to more extensive oligomerization of Re^I(dmp)(W)Zn^{II} than Re^I(dmp)(W)Cu^{II}, as indicated by longer rotation times, *ca*. 30 and 50 ns, respectively (see above). Oligomerization could shield the binding site and change its structure and energetics by intermolecular interactions. The energetic proximity of the ^{3}CT and ^{3}CS states contrasts with the ~0.4 V difference between the Re-label excited-state reduction potential (E' ≅ +1.4 V *vs*. NHE)[28] and the indole oxidation potential (E' ≅ 1.01 V)[54], suggesting that binding site energetics are strongly affected by the interaction between dmp indole groups and the protein environment.

The full potential of the Re^I(dmp)(W) ET phototrigger is revealed by the dramatic acceleration[9] of long-range Cu^I→Re^{II} ET in ^{3}CT-excited Re^I(dmp)(W)AzCu^I. Cu^{II} formation is complete in a few tens of ns, whereas no reaction is found for analogous azurins with phenylalanine or tyrosine at position 122. In the long-range ET mechanism of Re^I(dmp)(W)AzCu^I (Scheme 1), the rapidly established ^{3}CT / ^{3}CS equilibrium feeds the productive Cu^I→$W^{\bullet+}$ ET step from a long-lived ^{3}CT population, whereas ^{3}CS $dmp^{\bullet-}$→$W^{\bullet+}$ charge recombination is energy-wasting, decreasing the reaction yield. Productive Cu^I→$W^{\bullet+}$ ET is remarkably fast (31 ns) over a 1.12 nm distance, likely because the indole group is electronically well coupled with the peptide. The efficiency of any light-harvesting or photocatalytic system based on this type of mechanism will increase upon increasing the inherent ^{3}CT lifetime, slowing $dmp^{\bullet-}$→$W^{\bullet+}$ recombination and accelerating the final ET step.

The interaction between W(indole) and dmp is a prerequisite for rapid charge separation in Re^I(dmp)(W) through the ^{3}CT / ^{3}CS equilibrium. Indeed, W→Re^{II} ET is much slower in analogous systems without a direct indole-N,N contact. Photoinduced ET reactions in $[Re^I$(pyridine-W)$(CO)_3$(N,N)$]^+$ and $[Re^I$(imidazole-W)$(CO)_3$(N,N)$]^+$ (N,N =bpy, phen) occur with a time constant of ~30 ns in MeCN solutions, without any ultrafast kinetics component.[14, 51] Flash-quench-generated $Re^{II}(CO)_3$(phen)(H107) oxidizes W108 in Re(Q107H)(W48F/Y72F/H83Q/Y108W)AzZn^{II} with a 360 ns time constant,[34] much slower than the similar reaction in ^{3}CT-excited Re^I(dmp)(W)AzM. The phen and W108 indole rings in these modified proteins are oriented away from each other, disfavoring any direct electronic interaction.

Phototriggering by the Re^I(dmp)(W) unit in azurins is akin to the 30 ps primary electron transfer in DNA photolyase activation that occurs over ~1.5 nm, involving several ππ interactions: from the W382 indole group to an electronically excited flavin radical whose aromatic rings are partly overlapping 4.2 Å apart, followed by a sequence of ET steps through a "nanowire" of three π-π interacting tryptophans.[55-60] Ultrafast charge separation also is accomplished in a tight binding antibody protein pocket containing *t*-stilbene π-stacked to tryptophan. Stilbene photoexcitation produces a strongly luminescent ^{1}[$stilbene^{\bullet-}$/$W^{\bullet+}$] charge-separated complex with biosensing functions.[61] This type of ππ interaction also can mediate ET at protein-protein interfaces: fast equilibration between oxidized Zn-porphyrin and a nearby tryptophane has been demonstrated to facilitate charge recombination following photoexcitation of a Zn-cytochrome *c* peroxidase:cytochrome c complex.[62, 63]

We suggest that the principle underlying ET acceleration in Re^I(dmp)(W)AzM azurins, namely, ultrafast photoinduced charge separation between a π-stacked electron donor and acceptor, can guide the design and construction of more efficient light-energy harvesting systems. Rhenium carbonyl-diimine / tryptophan assemblies could be exploited in such constructions.

Supplementary Material

Refer to Web version on PubMed Central for supplementary material.

Acknowledgments

We thank Lucie Sokolová (J.W. Goethe University, Frankfurt am Main) for measuring and interpreting the solution LILBID mass spectra. Research at Caltech was supported by NSF Center for Chemical Innovation (Powering the Planet. CHE-0802907 and CHE-0947829) and by NIH (DK019038 to HBG, JRW). The crystallographic work was supported by NSF - CHE-0749997 (BRC). The TRIR and theoretical investigations were funded by the STFC Rutherford Appleton Laboratory, CMSD 43, Queen Mary University of London, European COST and ESF-DYNA programs, and Ministry of Education of the Czech Republic grants ME10124 and OC09043.

References

1. Langen R, Chang I-J, Germanas JP, Richards JH, Winkler JR, Gray HB. Science. 1995; 268:1733. [PubMed: 7792598]
2. Crane BR, Di Bilio AJ, Winkler JR, Gray HB. J Am Chem Soc. 2001; 123:11623. [PubMed: 11716717]
3. Di Bilio AJ, Hill MG, Bonander N, Karlsson BG, Villahermosa RM, Malmström BG, Winkler JR, Gray HB. J Am Chem Soc. 1997; 119:9921.
4. Skov LK, Pascher T, Winkler JR, Gray HB. J Am Chem Soc. 1998; 120:1102.
5. Gray HB, Winkler JR. Chem Phys Lett. 2009; 483:1. [PubMed: 20161522]
6. Grădinaru C, Crane BR. J Phys Chem B. 2006; 110:20073. [PubMed: 17034174]
7. Skourtis SS, Balabin IA, Kawatsu T, Beratan DN. Proc Natl Acad Sci USA. 2005; 102:3552–3557. [PubMed: 15738409]
8. Regan JJ, Onuchic JN. Adv Chem Phys. 1999; 107:497.
9. Shih C, Museth AK, Abrahamsson M, Blanco-Rodriguez AM, Di Bilio AJ, Sudhamsu J, Crane BR, Ronayne KL, Towrie M, Vlček A Jr, Richards JH, Winkler JR, Gray HB. Science. 2008; 320:1760. [PubMed: 18583608]
10. The *Pseudomonas aeruginosa* azurin mutants under study have a histidine (H) at position 124 and either tryptophan (W), tyrosine (Y), or phenylalanine (F) at position 122 on the β strand extending from methionine-121 that is coordinated to the metal atom (M = Cu^{I}, Cu^{II}, or Zn^{II}). All other tyrosines and tryptophans are replaced by phenylalanines, and the Re label $Re^{I}(CO)_3(dmp)$ (dmp = 4,7-dimethyl-1,10-phenanthroline) is bound to the H124 imidazole. These azurins are denoted Re^{I}(dmp)(A)AzM (A = W, Y, F). The symbol A also is used generically for an aromatic amino acid. Lysine (K) analogues used for comparison are denoted Re^{I}(dmp)(K)AzCu^{II} and Re^{I}(phen)(K)AzCu^{II} (phen = 1,10-phenanthroline).
11. Di Bilio AJ, Crane BR, Wehbi WA, Kiser CN, Abu-Omar MM, Carlos RM, Richards JH, Winkler JR, Gray HB. J Am Chem Soc. 2001; 123:3181. [PubMed: 11457048]
12. Towrie M, Grills DC, Dyer J, Weinstein JA, Matousek P, Barton R, Bailey PD, Subramaniam N, Kwok WM, Ma CS, Phillips D, Parker AW, George MW. Appl Spectrosc. 2003; 57:367. [PubMed: 14658632]
13. Vlček A Jr, Farrell IR, Liard DJ, Matousek P, Towrie M, Parker AW, Grills DC, George MW. J Chem Soc Dalton Trans. 2002:701.
14. Towrie M, Parker AW, Vlček A Jr, Gabrielsson A, Blanco Rodriguez AM. Applied Spectroscopy. 2005; 59:467. [PubMed: 15901332]
15. Blanco-Rodríguez AM, Busby M, Ronayne KL, Towrie M, Sýkora J, Hof M, Záliš S, Grădinaru C, Di Bilio AJ, Crane BR, Gray HB, Vlček A J. J Am Chem Soc. 2009; 131:11788. [PubMed: 19639996]
16. Cannizzo A, Blanco-Rodríguez AM, Nahhas A, Šebera J, Záliš S, Vlček A Jr, Chergui M. J Am Chem Soc. 2008; 130:8967. [PubMed: 18570416]
17. El Nahhas A, Cannizzo A, van Mourik F, Blanco-Rodríguez AM, Záliš S, Vlček A Jr, Chergui M. J Phys Chem A. 2010; 114:6361. [PubMed: 20465299]

18. Frisch, MJ.; Trucks, GW.; Schlegel, HB.; Scuseria, GE.; Robb, MA.; Cheeseman, JR.; Scalmani, G.; Barone, V.; Mennucci, B.; Petersson, GA.; Nakatsuji, H.; Caricato, M.; Li, X.; Hratchian, HP.; Izmaylov, AF.; Bloino, J.; Zheng, G.; Sonnenberg, JL.; Hada, M.; Ehara, M.; Toyota, K.; Fukuda, R.; Hasegawa, J.; Ishida, M.; Nakajima, T.; Honda, Y.; Kitao, O.; Nakai, H.; Vreven, T.; Montgomery, JA., Jr; Peralta, JE.; Ogliaro, F.; Bearpark, M.; Heyd, JJ.; Brothers, E.; Kudin, KN.; Staroverov, VN.; Kobayashi, R.; Normand, J.; Raghavachari, K.; Rendell, A.; Burant, JC.; Iyengar, SS.; Tomasi, J.; Cossi, M.; Rega, N.; Millam, JM.; Klene, M.; Knox, JE.; Cross, JB.; Bakken, V.; Adamo, C.; Jaramillo, J.; Gomperts, R.; Stratmann, RE.; Yazyev, O.; Austin, AJ.; Cammi, R.; Pomelli, C.; Ochterski, JW.; Martin, RL.; Morokuma, K.; Zakrzewski, VG.; Voth, GA.; Salvador, P.; Dannenberg, JJ.; Dapprich, S.; Daniels, AD.; Farkas, O.; Foresman, JB.; Ortiz, JV.; Cioslowski, J.; Fox, DJ. Gaussian 09, Revision A.02. Gaussian, Inc.; Wallingford CT: 2009.
19. Perdew JP, Burke K, Ernzerhof M. Phys Rev Lett. 1996; 77:3865. [PubMed: 10062328]
20. Adamo C, Barone V. J Chem Phys. 1999; 110:6158.
21. Zhao Y, Truhlar DG. Theor Chem Acc. 2008; 120:215.
22. Yanai T, Tew DP, Handy NC. Chem Phys Lett. 2004; 393:51.
23. Krishnan R, Binkley JS, Seeger R, Pople JA. J Chem Phys. 1980; 72:650.
24. Woon DE, Dunning TH Jr. J Chem Phys. 1993; 98:1358.
25. Andrae D, Häussermann U, Dolg M, Stoll H, Preuss H. Theor Chim Acta. 1990; 77:123.
26. Cossi M, Rega N, Scalmani G, Barone V. J Comput Chem. 2003; 24:669. [PubMed: 12666158]
27. Blanco-Rodríguez AM, Busby M, Grădinaru C, Crane BR, Di Bilio AJ, Matousek P, Towrie M, Leigh BS, Richards JH, Vlček A Jr, Gray HB. J Am Chem Soc. 2006; 128:4365. [PubMed: 16569013]
28. Connick WB, Di Bilio AJ, Hill MG, Winkler JR, Gray HB. Inorg Chim Acta. 1995; 240:169.
29. Lucia LA, Abboud K, Schanze KS. Inorg Chem. 1997; 36:6224.
30. Busby M, Matousek P, Towrie M, Clark IP, Motevalli M, Hartl F, Vlček A Jr. Inorg Chem. 2004; 43:4523. [PubMed: 15236567]
31. Liard DJ, Busby M, Farrell IR, Matousek P, Towrie M, Vlček A Jr. J Phys Chem A. 2004; 108:556.
32. Busby M, Gabrielsson A, Matousek P, Towrie M, Di Bilio AJ, Gray HB, Vlček A Jr. Inorg Chem. 2004; 43:4994. [PubMed: 15285676]
33. Wallace L, Woods C, Rillema DP. Inorg Chem. 1995; 34:2875.
34. Miller JE, Gradinaru C, Crane BR, Di Bilio AJ, Wehbi WA, Un S, Winkler JR, Gray HB. J Am Chem Soc. 2003; 125:14220. [PubMed: 14624538]
35. Dattelbaum DM, Omberg KM, Schoonover JR, Martin RL, Meyer TJ. Inorg Chem. 2002; 41:6071. [PubMed: 12425635]
36. Bredenbeck J, Helbing J, Hamm P. J Am Chem Soc. 2004; 126:990. [PubMed: 14746445]
37. Sokolová L, Williamson H, Sýkora J, Hof M, Gray HB, Brutschy B, Vlček A Jr. manuscript in preparation.
38. Dattelbaum DM, Omberg KM, Hay PJ, Gebhart NL, Martin RL, Schoonover JR, Meyer TJ. J Phys Chem A. 2004; 108:3527.
39. George MW, Johnson FPA, Westwell JR, Hodges PM, Turner JJ. J Chem Soc Dalton Trans. 1993:2977.
40. Gamelin DR, George MW, Glyn P, Grevels F-W, Johnson FPA, Klotzbücher W, Morrison SL, Russell G, Schaffner K, Turner JJ. Inorg Chem. 1994; 33:3246.
41. Vlček A Jr. Topics Organomet Chem. 2010; 29:73.
42. Vlček A Jr, Záliš S. Coord Chem Rev. 2007; 251:258.
43. Liard DJ, Busby M, Matousek P, Towrie M, Vlček A Jr. J Phys Chem A. 2004; 108:2363.
44. Hansen JE, Longworth JW, Fleming GR. Biochemistry. 1990; 29:7329. [PubMed: 2119804]
45. Wolcan E, Alessandrini JL, Féliz MR. J Phys Chem B. 2005; 109:22890. [PubMed: 16853982]
46. Knight TE, McCusker JK. J Am Chem Soc. 2010; 132:2208–2221. [PubMed: 20104841]
47. Johnson FPA, George MW, Hartl F, Turner JJ. Organometallics. 1996; 15:3374.

48. Gabrielsson A, Hartl F, Zhang H, Lindsay Smith JR, Towrie M, Vlček A Jr, Perutz RN. J Am Chem Soc. 2006; 128:4253. [PubMed: 16569000]
49. Stor GJ, Hartl F, van Outersterp JWM, Stufkens DJ. Organometallics. 1995; 14:1115.
50. Lewis JD, Towrie M, Moore JN. J Phys Chem A. 2008; 112:3852. [PubMed: 18393475]
51. Blanco-Rodríguez AM, Towrie M, Záliš S, Sýkora J, Vlček A Jr. manuscript in preparation.
52. Aubert C, Vos MH, Mathis P, Eker APM, Brettel K. Nature. 2000; 405:586. [PubMed: 10850720]
53. El Nahhas A, Consani C, Blanco-Rodríguez AM, Lancaster KM, Braem O, Cannizzo A, Towrie M, Clark IP, Záliš S, Chergui M, Vlček A Jr. Inorg Chem. 2011 manuscript in preparation.
54. Harriman A. J Phys Chem. 1987; 91:6102.
55. Lukacs A, Eker APM, Byrdin M, Brettel K, Vos MH. J Am Chem Soc. 2008; 130:14394. [PubMed: 18850708]
56. Byrdin M, Eker APM, Vos MH, Brettel K. Proc Natl Acad Sci USA. 2003; 100:8676–8681. [PubMed: 12835419]
57. Byrdin M, Lukacs A, Thiagarajan V, Eker APM, Brettel K, Vos MH. J Phys Chem A. 2010; 114:3207–3214. [PubMed: 19954157]
58. Lukacs A, Eker APM, Byrdin M, Villette S, Pan J, Brettel K, Vos MH. J Phys Chem B. 2006; 110:15654. [PubMed: 16898706]
59. Tanaka F, Chosrowjan H, Taniguchi S, Mataga N, Sato K, Nishina Y, Kiyoshi Shiga K. J Phys Chem B. 2007; 111:5694. [PubMed: 17474766]
60. Park H-W, Kim S-T, Sancar A, Deisenhofer J. Science. 1995; 268:1866. [PubMed: 7604260]
61. Debler EW, Kaufmann GF, Meijler MM, Heine A, Mee JM, Pljevaljcic G, Di Bilio AJ, Schultz PG, Millar DP, Janda KD, Wilson IA, Gray HB, Lerner RA. Science. 2008; 319:1232. [PubMed: 18309081]
62. Seifert JL, Pfister TD, Nocek JM, Lu Y, Hoffman BM. J Am Chem Soc. 2005; 127:5750. [PubMed: 15839648]
63. Kang SA, Crane BR. Proc Natl Acad Sci USA. 2005; 102:15465–15470. [PubMed: 16227441]

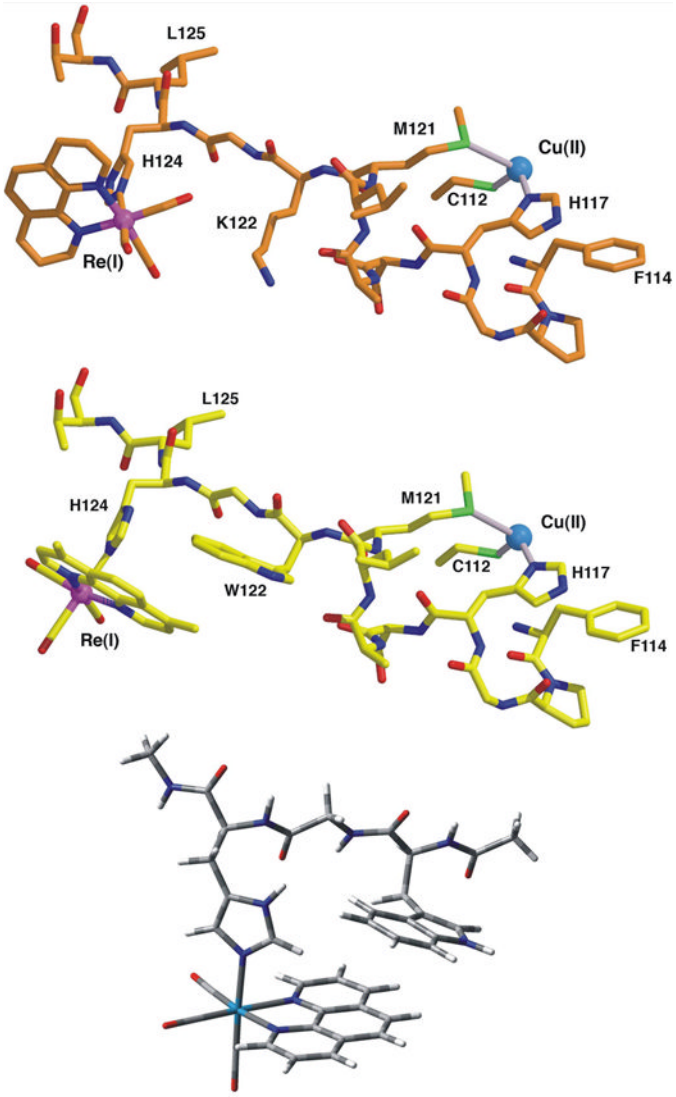

Figure 1.

Fragments of the Re^{I}(phen)(K)AzCu^{II} (top) and Re^{I}(dmp)(W)AzCu^{II} (middle) crystal structures showing the $Re(CO)_3$(N,N) label attached to the imidazole group of H124 and the peptide link to the Cu atom.[9, 15] Bottom: Optimized structure of the $[Re^{I}(phen)(W)]^{+}$ unit used in DFT and TDDFT calculations.

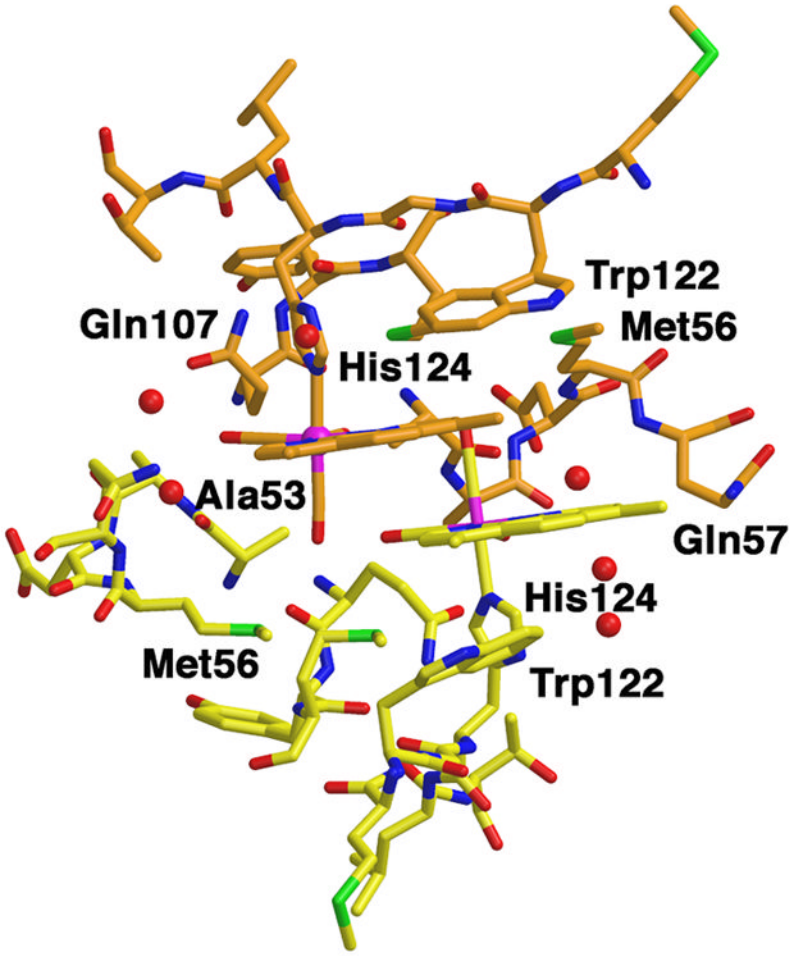

Figure 2.
Structure of Re^{I}(dmp)(W)AzCu^{II} in the metallolabel region.
The red spheres represent water molecules.

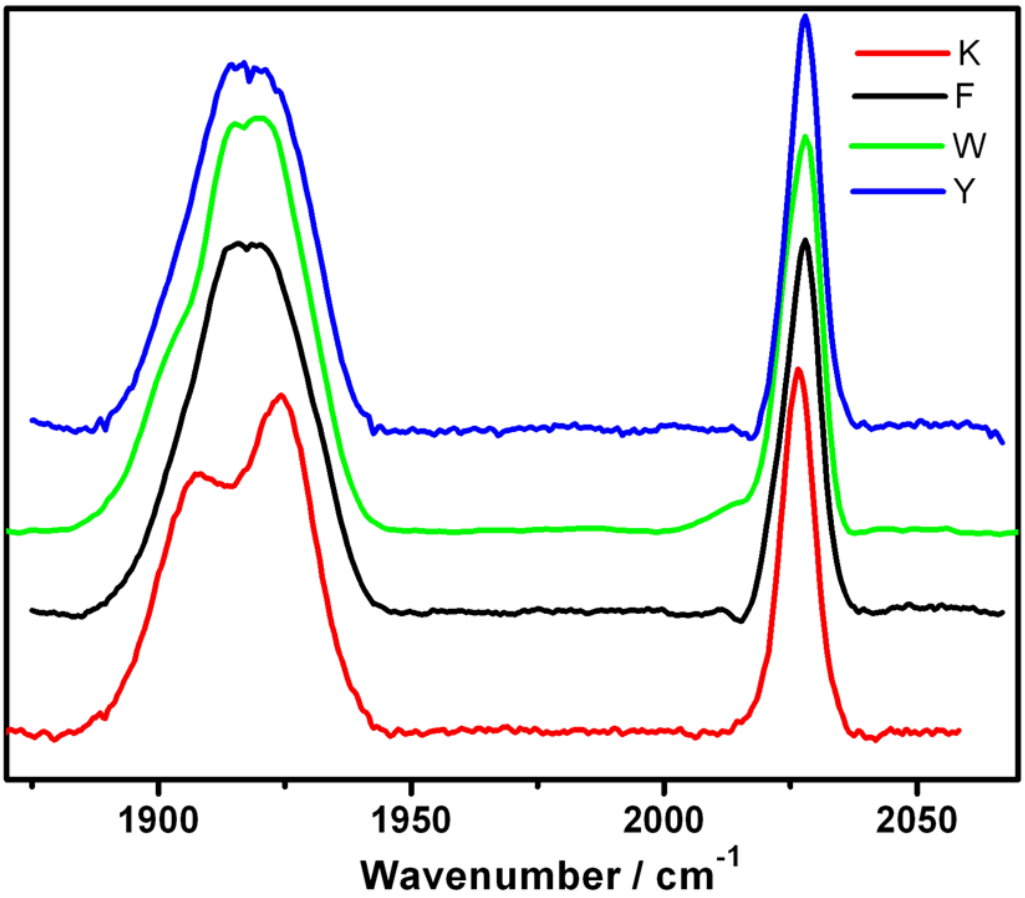

Figure 3.
Ground-state FTIR spectra of Re^{I}(dmp)(A)AzCu^{II} (A = W, F), Re^{I}(dmp)(Y)AzZn^{II} (Y) and Re^{I}(phen)(K)AzCu^{II} (K) in a KP_i (D_2O, pD ~ 7.1) buffer.

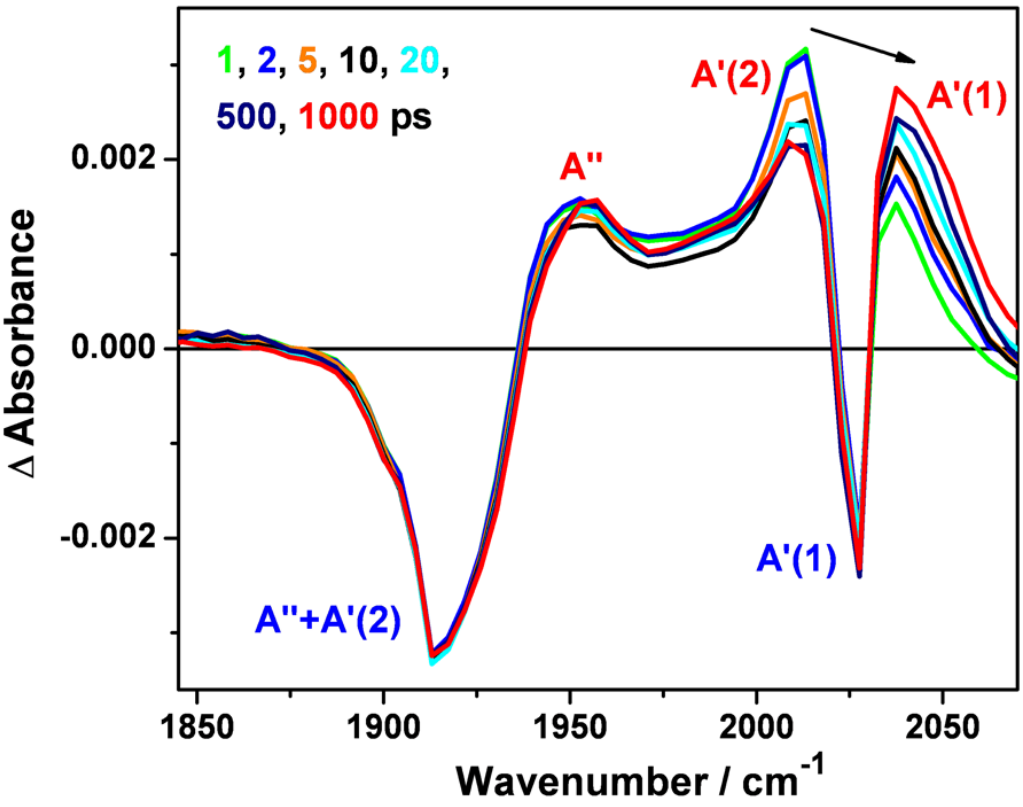

Figure 4.

Picosecond TRIR spectra of $Re^{I}(dmp)(Y)AzZn^{II}$ measured at selected time delays after 400 nm, ~150 fs excitation. Positive and negative bands correspond to excited-state and bleached ground-state absorptions, respectively. The experimental points are separated by 4-5 cm^{-1}. The black arrow shows the dynamical evolution of the excited-state A'(1) band shifting with time from about ~2014 to ~2039 cm^{-1}. The ground-state band occurs at 2029 cm^{-1}. Virtually identical TRIR spectra were obtained for 1.9 mM solutions of $Re^{I}(dmp)(Y)AzCu^{II}$ and $Re^{I}(dmp)(F)AzCu^{II}$ in 50 mM KP_i buffer in D_2O (pD ~7.0) at 21 °C. See Figure S1 for the ns TRIR.

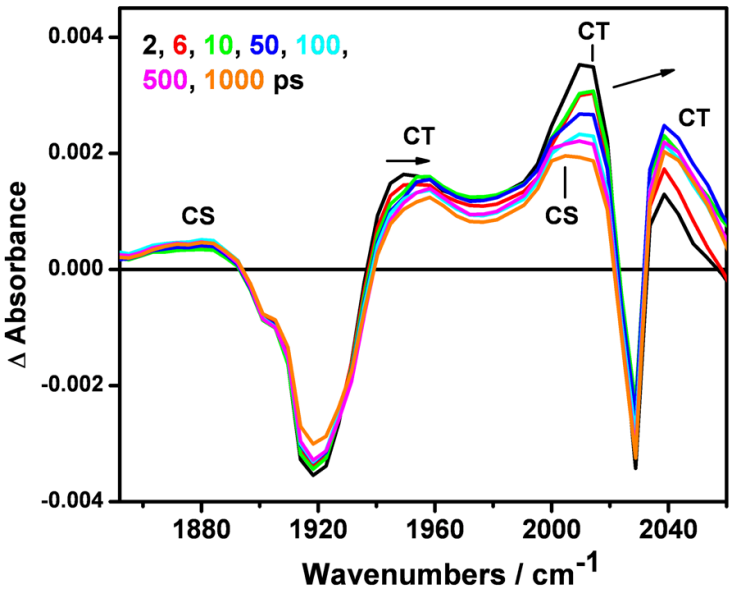

Figure 5.

Picosecond TRIR spectra of $Re^{I}(dmp)(W)AzZn^{II}$ measured at selected time delays (in ps) after 400 nm, ~150 fs excitation. Experimental points are separated by 4-5 cm^{-1}. The arrows show the relaxation-related ^{3}CT band shifts (the small ^{3}CS rise is apparent only after background subtraction). Solution in 50 mM KPi buffer in D_2O (pD ~7.0) at 21 °C.

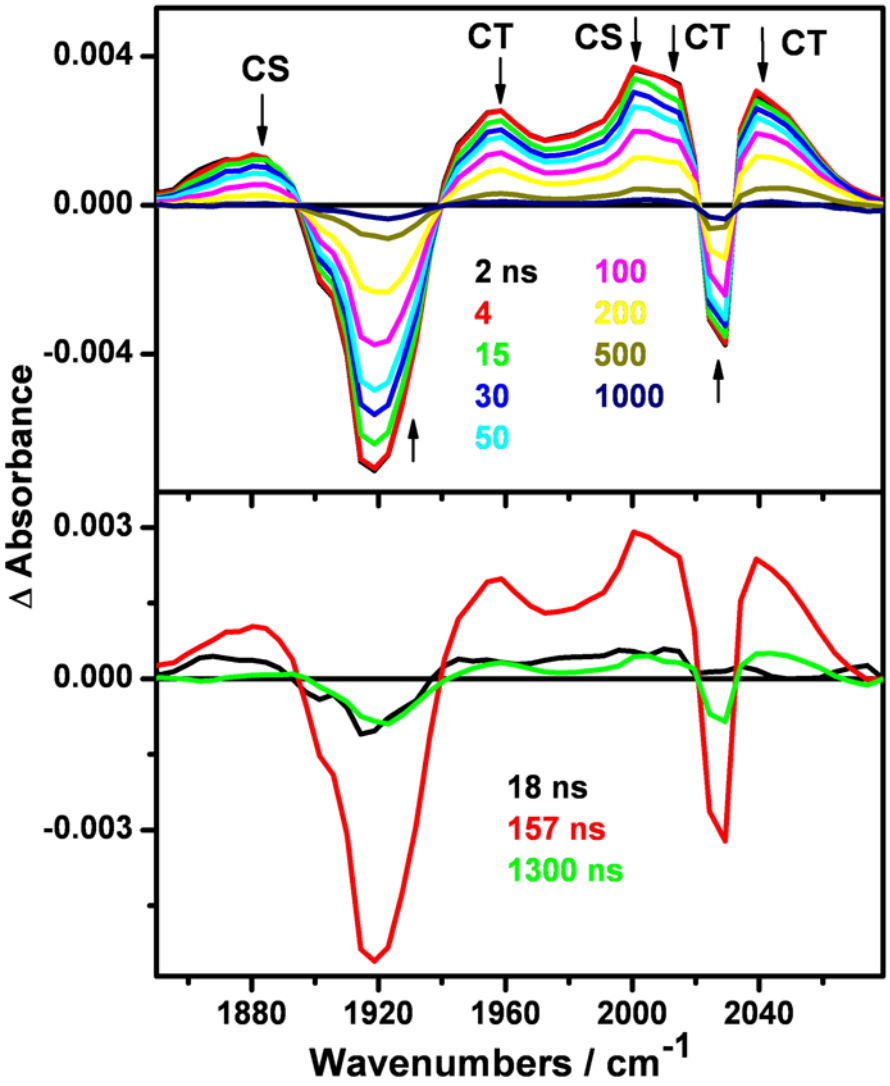

Figure 6.

Top: Nanosecond TRIR spectra of 4.4 mM Re^{I}(dmp)(W)AzZn^{II} measured at selected time delays (in ns) after 355 nm, ~0.7 ns excitation. Experimental points are separated by 4-5 cm^{-1}. Bottom: DAS obtained by SVD/global fitting. The 1300 ns lifetime was fixed in the analysis, based on Re^{I}(dmp)(Y)AzZn^{II} emission decay. The spectra evolve in the direction of the arrows. Solution in 50 mM KP_i buffer in D_2O (pD ~7.0) at 21 °C.

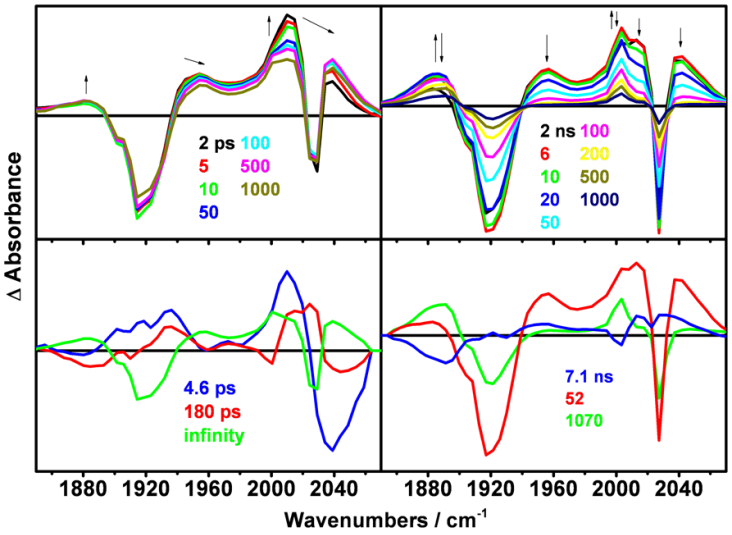

Figure 7.

Top: TRIR spectra of $Re^{I}(dmp)(W)AzCu^{II}$ measured in the ps time range after 400 nm, ~150 fs excitation (left panel) and the ns range after 355 nm, ~0.7 ns excitation (right panel). The spectra evolve in the direction of the arrows. Bottom: DAS spectra corresponding to kinetics components of 4.6±1.1, and 180±90 ps (left panel); 7.1±1, 52.3±6.5, and 1069±142 ns (right panel). The "infinity" DAS results from extrapolation of the ps measurement to long time delays, approximately corresponding to an early-ns spectrum. Solution in 50 mM KP_i buffer in D_2O (pD ~7.0) at 21 °C.

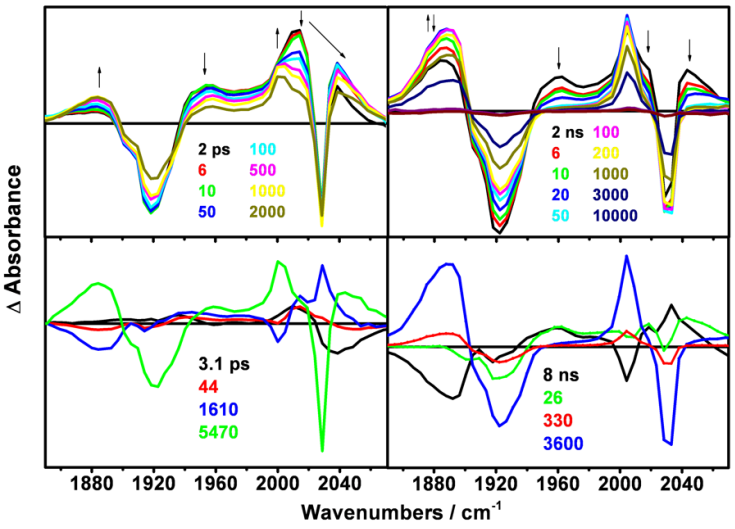

Figure 8.

Top: TRIR spectra of Re^{I}(dmp)(W)AzCu^{I} measured in the ps time range after 400 nm, ~150 fs excitation (left panel) and the ns range after 355 nm, ~0.7 ns excitation (right panel). Bottom: DAS spectra corresponding to kinetics components specified in Table 1. The 5470 ps DAS (bottom left, green) results from extrapolation to long time delays, approximately corresponding to an early-ns spectrum.

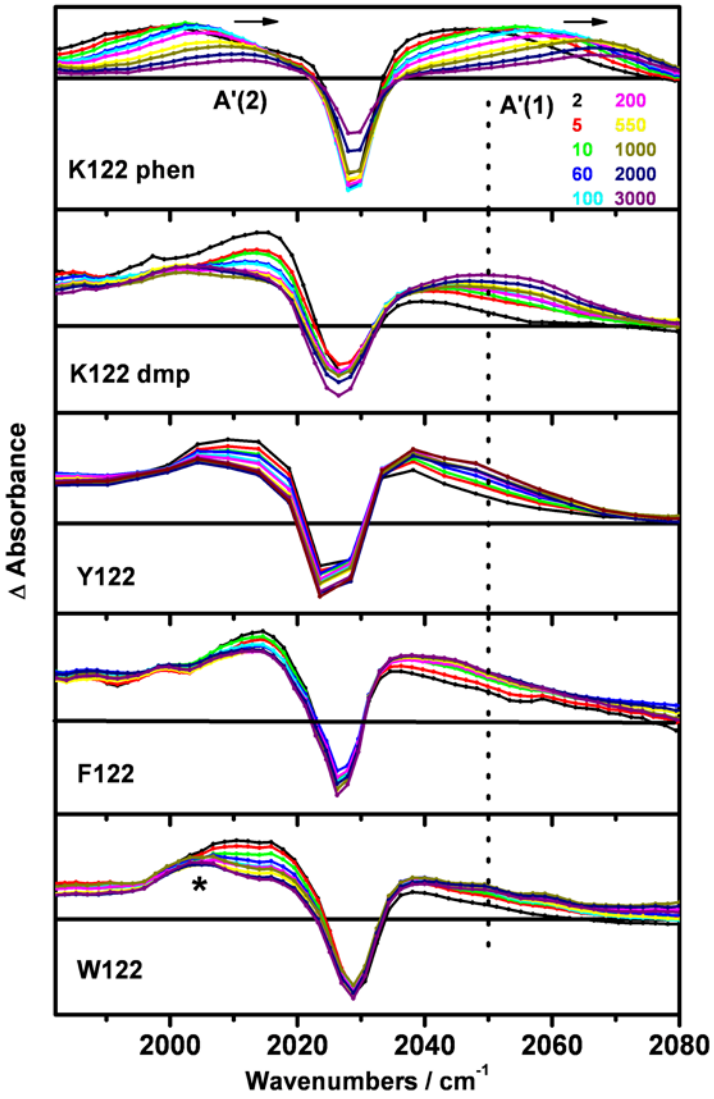

Figure 9.

Time-resolved IR spectra of Re(N,N)(A)-labeled azurins in the high-energy part of the ν(CO) region. From top to bottom: Re(phen)(K)AzCu^{II}, Re(dmp)(K)AzCu^{II}, Re^{I}(dmp)(Y)AzCu^{II}, Re^{I}(dmp)(F)AzCu^{II}, and Re^{I}(dmp)(W)AzCu^{II} (3-4 mM in KP$_i$-D$_2$O, pD ~ 7.1, 21 °C) measured at selected time delays (see the top panel) after 400 nm, ~150 fs laser-pulse excitation. The dotted line shows the position of the highest excited-state band of Re^{I}(dmp)(K)AzCu^{II}. Experimental points are separated by ~5 cm^{-1} for Re^{I}(dmp)(Y)AzCu^{II} and ~1.9 cm^{-1} for all others.

*: spectral feature due to the ^{3}CS formation.

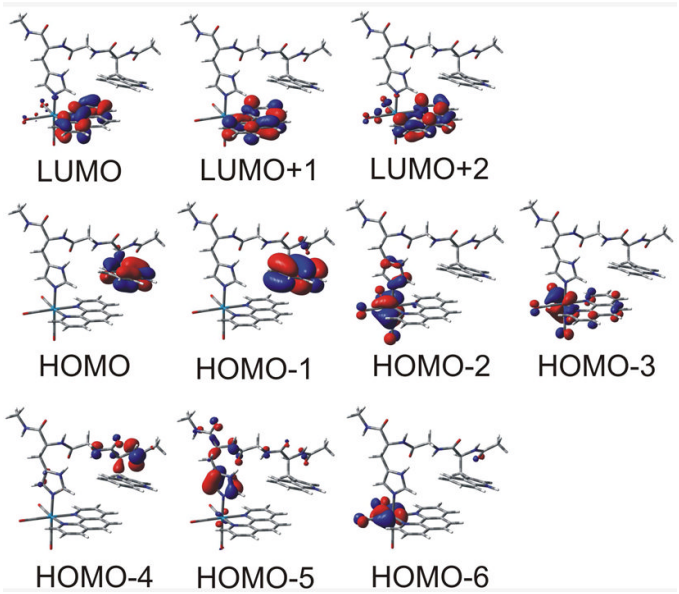

Figure 10.
Frontier molecular orbitals of the $[Re^{I}(phen)(W)]^{+}$ fragment calculated by DFT (PBE0, CPCM-H_2O)

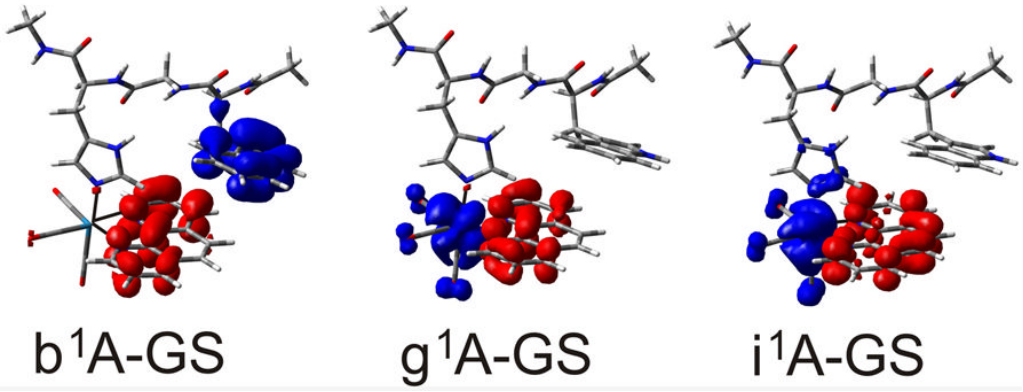

Figure 11.
TDDFT (PBE0, CPCM-H_2O) calculated electron density difference between the lowest W(indole)→phen ^{1}CT state (left, b^{1}A) and the two optically populated ^{1}CT states (g^{1}A and i^{1}A, Table S2) and the [Re^I(phen)(W)]$^+$ ground state. Colors show regions where the electron density decreases (blue) and increases (red) upon excitation.

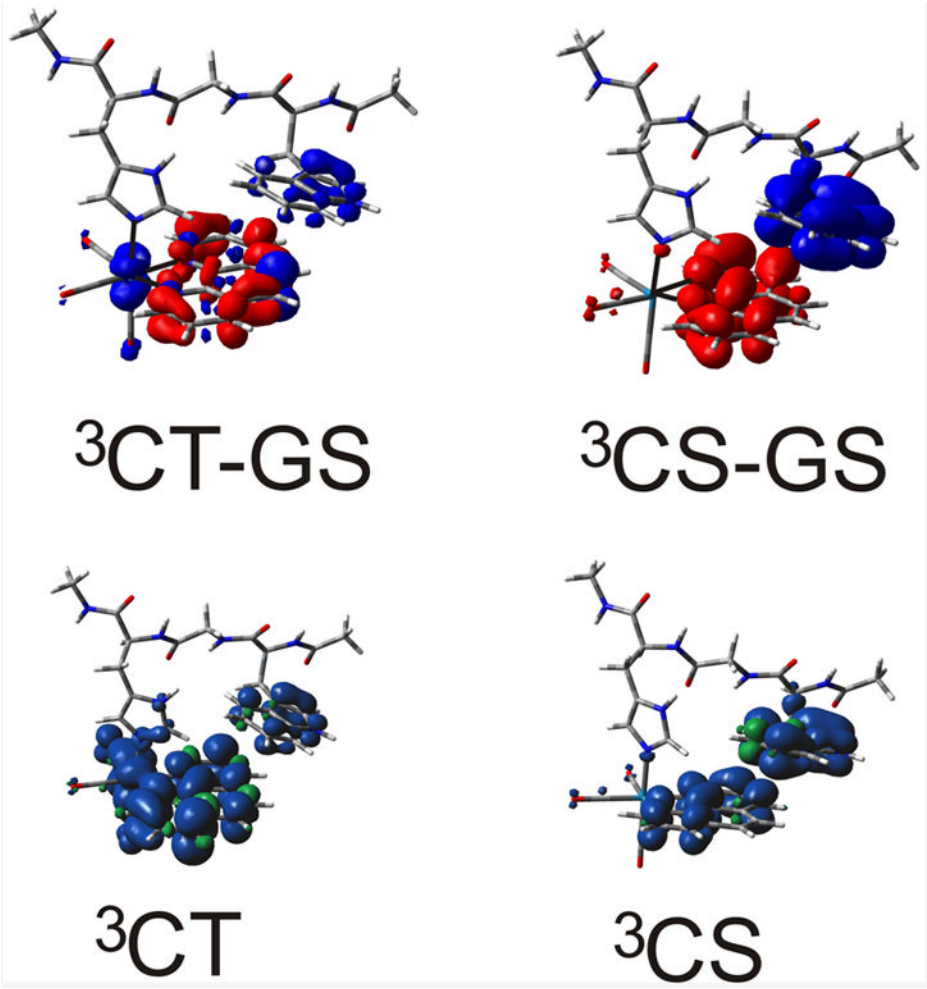

Figure 12.

Top: Electron density differences between ^{3}CT and ^{3}CS states and the ground state at the ground-state geometry calculated by TD-DFT (CPCM-H_2O). Bottom: spin density distributions in structurally optimized ^{3}CT and ^{3}CS states (DFT UKS CPCM-H_2O). PBE0 and M06 functionals were used for the ^{3}CT and ^{3}CS calculations, respectively.

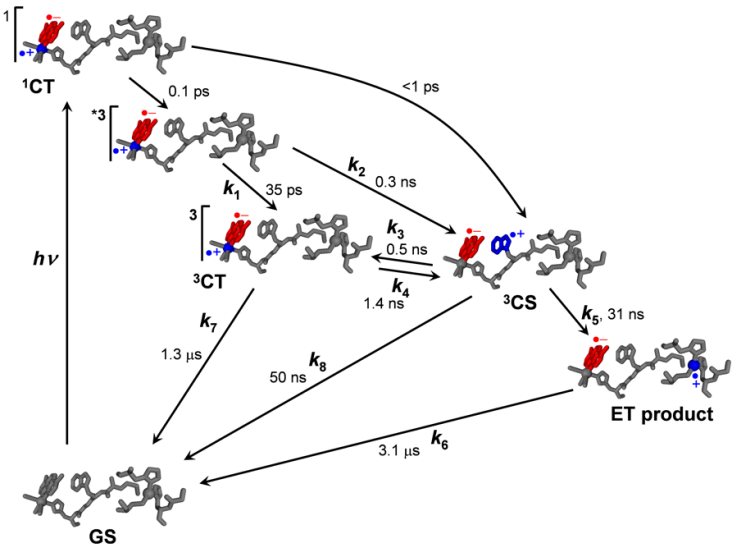

Scheme 1.

Photoinduced electron transfer through Re^{I}(dmp)(W)AzCu^{I}. Optical population of several ^{1}CT excited states is followed by a series of relaxation and ET steps. The sites of the excited electron and hole are shown in red and blue, respectively. Lifetime values[9] are pertinent to Re^{I}(dmp)(W)AzCu^{I}.

Table 1

Exponential time constants of TRIR spectral evolution and emission decay of Re(dmp)(W)AzM. Kinetics data obtained from solutions in 50 mM KP_i buffer in D_2O (pD ~7.0) at 21 °C.

Re(dmp)(W)AzM	M = Zn^{II}	M = Cu^{II}	M = Cu^{II} emission[c]	M = Cu^{I} Alternative TRIR	M = Cu^{I} emission[e]
ultrafast CS rise / CT decay	<1 ps	<1 ps		<1ps	
relaxation[a]	-	4-5 ps		3-4 ps	
CS rise / CT decay relaxation	≤50 ps	100-270 ps	2.9±0.1 ns[d]	40-100 ps	350 ps
CS rise / CT decay	-	4-8 ns	19±1 ns	1.6 ns	
CS rise / CT decay	-	-	-	8±1.6 ns	
CS rise / CT decay	-	-	-	27±7 ns	25 ns
CS + CT decay	18±4 ns 157±7 ns[a]	40-60 ns	63±1 ns	-	
CS decay		1.0-1.5 μs[b]		330±172 ns 3.6±0.3 μs	

[a] Additional very weak ^{3}CT signal is present, decaing with τ of 1.3 μs.

[b] Very weak residual signal.

[c] 1.9 mM solution in H_2O, 50 mM NaP_i (pH ≅7.1).

[d] Likely due to dynamic Stokes shift.

[e] From ref. 9.